university of groningen / faculty of science and engineering

Molecular Shape of Semi-flexible Bottlebrush Polymers

Cristina Cacace

S5756626

Faculty of Science and Engineering

Period: 25 Apr 2024 - 01 Jul 2024

Internship

Supervisor: PhD Andrea Giuntoli, Faculty of Science and Engineering

Examiner: PhD Andrea Giuntoli, Faculty of Science and Engineering

Contents

Page

1 Introduction **4**

2 Background Literature **6**
2.1 Structural parameters and Conformational properties of BBPs 6
2.2 Scaling Laws 7
2.2.1 Dependence of Radius of Gyration on Backbone Length 7
2.2.2 Dependence of Persistence Length and Side chain Length 8

3 Methods **11**
3.1 Molecular Dynamics 11
3.2 Model 12
3.3 Analysis 13

4 Results and Discussion **14**
4.1 Radius of Gyration in Semi-flexible Bottlebrush Polymers 15
4.2 Persistence Length in Semi-flexible Bottlebrush Polymers 15

5 Conclusion **18**

Bibliography **19**

Abstract

Bottlebrush polymers (BBPs) are a category of branched polymers that have drawn much interest in polymer science due to their diverse range of applications. The properties of these polymers can be modified by adjusting architectural parameters such as grafting density and the degree of polymerization of the side chains and backbone. For this reason, a significant number of experimental and computational studies have been carried out to investigate the conformations of BBPs under various conditions. This study explores the conformational properties and static structure of flexible and semi-flexible bottlebrush polymers in dilute solutions using molecular dynamics simulations with a coarse-grained model. Specifically, semi-flexible polymers are of particular interest due to their unique mechanical and structural behaviors, which remain underexplored in current research. We investigate the key dependencies between conformational properties and structural parameters, particularly focusing on the radius of gyration and the persistence length as functions of varying degrees of polymerization and stiffness. The results reveal a strong correlation between the radius of gyration and increasing backbone length N_b, which is further affected by the introduction of polymer stiffness. Through the analysis of the bond correlation function $C(x)$, we also demonstrate that higher stiffness values result in larger persistence lengths, indicating that stiffer polymers maintain their directional orientation over greater distances. These findings confirm theoretical predictions and align with experimental observations, providing valuable insights into the impact of structural modifications on the behavior of bottlebrush polymers.

1 Introduction

Bottlebrush polymers (BBPs) have attracted much attention in polymer science for being versatile macromolecules due to their unique combination of molecular and particulate characteristics, which are crucial in both biological and synthetic contexts [24]. These intriguing polymers are highly sought after for the development of advanced materials with improved or new properties, such as templates, elastomers, organic optoelectronic materials, and energy storage solutions, to name but a few [18]. They also hold promise for biomedical applications such as drug delivery, imaging, and biodetection [34].

Bottebrush polymers structural features are inspired by the intricate design of proteoglycans, which regulate essential functions in human body such as joint lubrication and clearance of lungs [12, 15]. BBPs represent an important category of high-density side-chain-grafted polymers. Characterized by high molecular weights (MWs), these structures consist of one or more polymeric side chains attached to each repeating unit of a linear polymer backbone, giving them a distinctive ”bottlebrush” morphology as shown in Figure 1. Depending on the substrates they are attached to, polymer brushes can exhibit one-dimensional (1D), two-dimensional (2D), and three-dimensional (3D) characteristics [28]. Specifically, the term ”bottlebrush polymer” or ”molecular bottlebrush” refers to a 1D polymer brush with an ultrahigh sidechain grafting density on a linear polymer backbone. Alternatively, for 1D polymer brushes with relatively sparse sidechain grafts, the terms ”graft copolymer” or ”comb-like polymer” are commonly used.

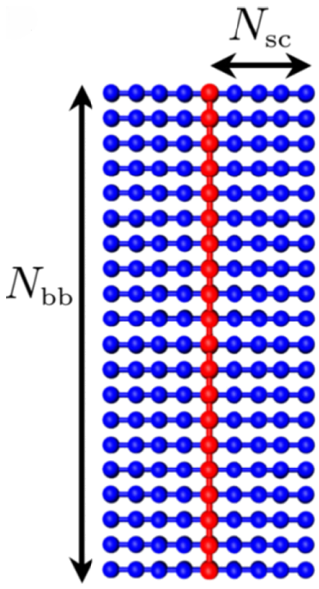

Figure 1: The architecture of a bottlebrush molecule, featuring a backbone composed of N_{bb} monomers (red beads) and sidechains made of N_{sc} monomers (blue beads) [24].

Important progress in polymerization methods now permit the synthesis of these hyperbranched molecules with meticulously managed structures. BBPs exhibit diverse architectures (Figure 3), categorized by the orientation of their backbone and side chains, as well as grafting densities, which allows for exceptional performance across various potential applications. Fine-tuning BBPs conformations and properties for specific purposes involves manipulating structural and environmental parameters such as solvent, temperature, pH, and salt concentration [20].
Experimentally, it is challenging to determine the relationship between microscopic conformational

details and the molecular-level properties of polymers, especially at short time scales (below 10 nanoseconds), due to limitations in resolution. This challenge highlights the attractiveness of computational approaches [20]. For bottlebrush polymers (BBPs), these microscopic details often encompass grafting density, backbone length, and side chain lengths, among others. These characteristics are crucial for depicting the conformation of such polymers. Given their importance, this study will specifically investigate how the spatial arrangement of BBPs is influenced by architectural parameters, with a particular focus on the effects of introducing chain rigidity, thereby transforming these polymers into semi-flexible bottlebrush polymers.

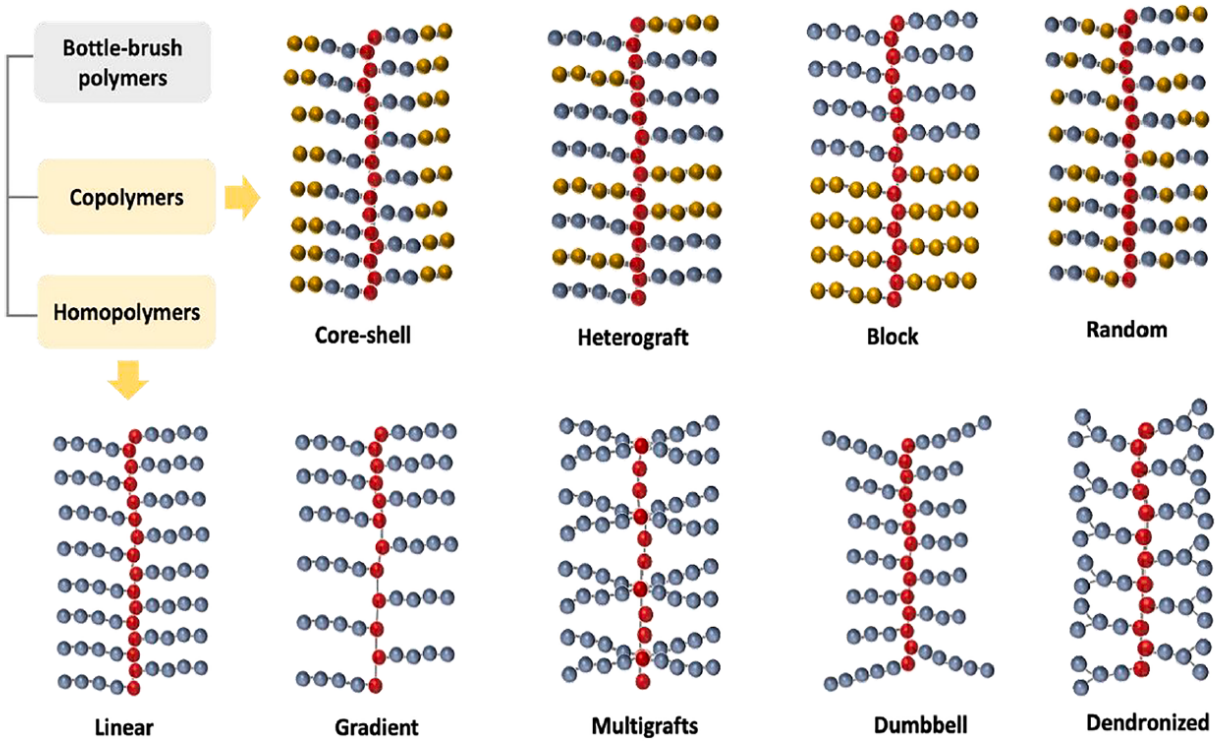

Figure 2: Different branching topologies of bottlebrush polymers [20].

Important biological macromolecules, such as aggrecans, resemble bottlebrushes but present additional complexities, such as semi-flexible polymer chains, electrostatic interactions, and a high degree of polydispersity [22]. Current bottlebrush models do not fully capture these effects, making it essential to extend our understanding to a wider class of bottlebrush-like molecules through computational studies.

In this work, we conducted simulations to examine the conformational properties of semi-flexible BBPs by varying parameters such as backbone length and sidechain length, and analyzing how these modifications affect the radius of gyration and the persistence length. Our findings reveal that increasing the rigidity of the polymer backbone significantly affects the local conformation, such as the persistence length, and the overall conformation of BBPs, such as the radius of gyration.

The relevance of this work lies in its potential to enhance the design and application of BBPs in both synthetic and biological fields, leading to the development of materials with tailored properties for specific applications.

2 Background Literature

In this chapter, we will investigate the qualitative and quantitative relationships between the conformational parameters and structural parameters of bottlebrush polymers.

2.1 Structural parameters and Conformational properties of BBPs

The structural parameters encompass the degree of polymerization of the backbone (N_b), the degree of polymerization of the grafted sidechain (N_g), and the degree of polymerization of the subchain between neighboring branch points (Ns), with the graft density of the sidechain (σ) being the reciprocal of Ns, i.e., $\sigma = \mathrm{N_s}^{-1}$ which quantifies the number of grafts per backbone unit.
The conformational characteristics of polymers chains can be categorized into two types: global and local properties (see Figure 3). The general conformational properties consist of the radius of gyration (R_g), the end-to-end distance of the backbone ($R_{e,b}$), the contour length (L_c), and the section diameter (D). Local conformational characteristics include the end-to-end distance of the sidechain ($R_{e,g}$), the spacing between adjacent grafting points (h), the persistence length (l_p) and the length of a Kuhn monomer (b). As σ rises, the increased excluded volume interactions cause a conformational shift from a random coil to a sparse comb-like structure, eventually forming a bottlebrush conformation, primarily due to the increased local crowding [36].
The polymer scientific community has shown considerable interest in the relationship between the average conformation of comb-like chains in dilute solution and the structural parameters, i.e., scaling laws, due to its importance in advancements across many fields. However, there is a gap in comprehensive reviews that specifically address the structure and conformation parameters of comb-like chains at the single macromolecule level. This gap highlights the necessity for systematic studies to better understand these fundamental aspects, which are essential for optimizing the performance of comb-like polymers in practical applications [36].

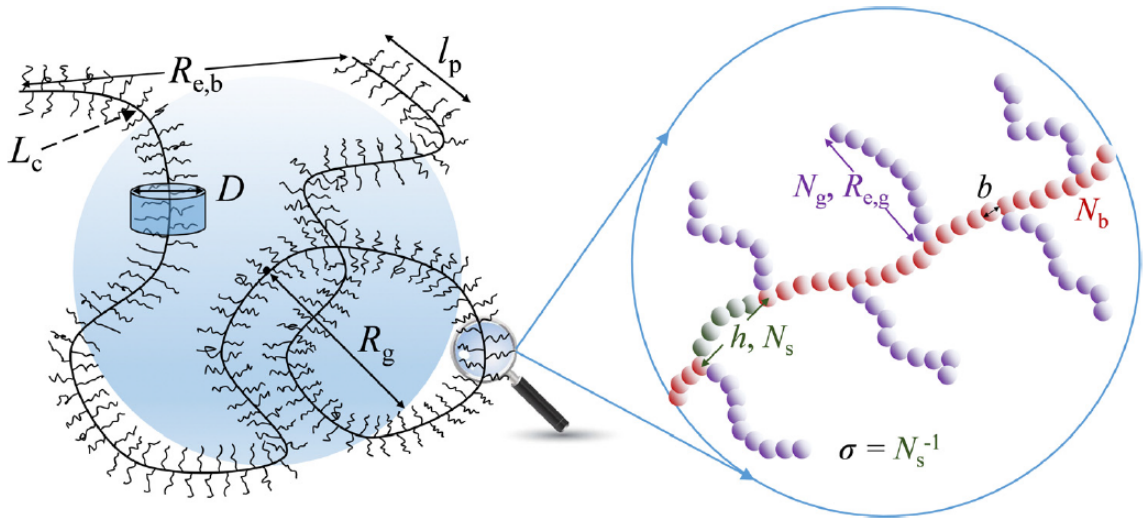

Figure 3: Schematic representations of the structural parameters and conformational properties of comb-like polymer chains [36].

2.2 Scaling Laws

Scaling theories are an effective method for translating the characteristics of complex systems into simple relationships, linking certain microscopic elements to a set of general attributes.
According to Flory's theory [27], there exists a universal power law dependence between the polymer size R and the number of monomers N for linear chains:

$$R \propto N^{\alpha} \tag{1}$$

where the exponent α depends on solvent conditions and is typically 0.588 for linear chains.
However, for branched polymers such as comb-like chains, the exponent α will differ due to the presence of branching. The specific value of α for branched polymers depends on the degree and type of ramifications. Therefore, it is essential to consider the effects of branching when applying scaling laws to these systems. We are going to take into consideration good solvent conditions, where monomers are separated by solvent molecules. The significant qualitative and quantitative relationships between conformational properties and structural parameters of (comb-like) polymers were examined in different studies from three perspectives: theoretical prediction, experimental verification, and computational simulation. From this progress, several general observations can be made.

2.2.1 Dependence of Radius of Gyration on Backbone Length

Studying how the conformational property depends on the backbone length is essential to explore the influence of other structural parameters. In polymer physics, the radius of gyration is used to describe the dimensions of a polymer chain. The square radius of gyration is defined as the average squared distance between the monomers in a given conformation (position vector $\mathbf{R}_i$) and the polymer's center of mass (position vector $\mathbf{R}_{\mathrm{cm}}$) [27]:

$$R_g^2 = \frac{1}{N}\sum_{i=1}^{N}(\mathbf{R}_i - \mathbf{R}_{\mathrm{cm}})^2 \tag{2}$$

Most research examines the dependence of R_g on N_b while keeping N_g constant, implying that varying N_b does not affect local stiffness and other local characteristics.
Simulation snapshots shown in Figure 4 illustrate the changes in chain conformation with increasing N_b. Their coarse-grained bead-spring model revealed that as N_b increases, the conformation transitions from star-like to elongated (around $N_b = 87$ for both Ng shown) and eventually to a coil-like shape. These transitions vary slightly with different N_g values, especially around $N_b = 87$ and 175, indicating that longer sidechains can create a marginally stiffer structure [7].
Additionally, several studies [8, 35] have investigated the relationship between the radius of gyration (R_g) and the backbone length (N_b) using Monte Carlo simulations. They observed that, while varying N_b with constant N_g, the exponent α in the relation $R_g \propto N_b^{\alpha}$ typically falls in the range of 0.6-0.7, showing minimal dependence on graft density. This relationship is illustrated in Figure 5, where the slope of 1.23 represents the relationship between R_g^2 and N_b, confirming the 0.6-0.7 range for α.
Overall, theoretical, experimental, and simulation studies consistently agree in placing α in the 0.6 to 0.7 range, demonstrating the strong relationship between R_g and N_b.

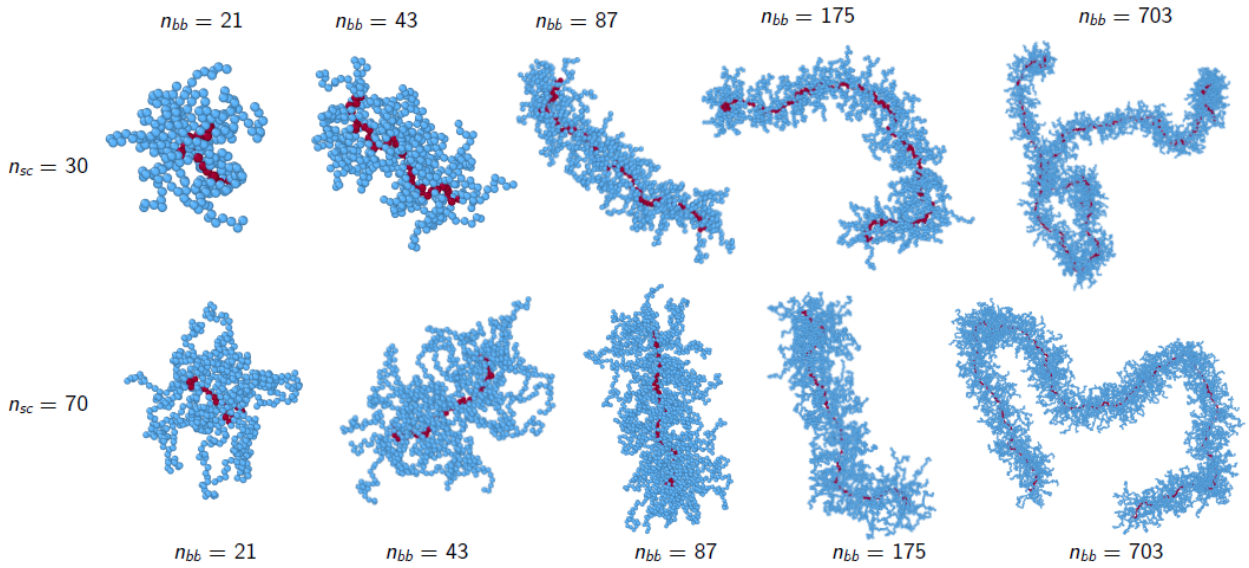

Figure 4: Simulation snapshots of a bottlebrush with varying backbone lengths for two kinds of sidechain ($N_g = 30$ and 70), where n_{sc} and n_{bb} represent N_g and N_b in the original paper, respectively [7].

2.2.2 Dependence of Persistence Length and Side chain Length

Bottlebrush polymers are typically synthesized by polymerizing an end-functionalized macromonomer [18], resulting in a structure where each backbone monomer carries a sidechain, leaving no flexible spacer between adjacent branches. When the backbone has sufficiently long sidechains, the polymer exhibits significant rigidity, characterized by an increased persistence length, despite the inherent flexibility of its chemical components. This rigidity arises from the excluded-volume interactions between the side chains, making it dependent on their length [8]. The persistence length l_p is an importance measure of the stiffness of the polymer backbone and several definitions have been proposed in the literature.

The persistence length is the distance over which the tangent direction of the polymer chain loses its correlation. Formally, it is [10] defined as the average projection of $\mathbf{R}$ on an interior bond vector $\mathbf{u}_{\mathrm{in}}$, far from any chain ends. The classical definitions of persistence length involve projecting the end-to-end vector, $\mathbf{R}$, onto a bond vector and averaging this over all possible conformations. Specifically [35],

$$l_k = \langle \mathbf{R} \cdot \mathbf{u}_k \rangle \tag{3}$$

where $\mathbf{u}_k$ is the normalized bond vector between sites k and $k+1$. Another way to define the persistence length is through the bond angle correlation function, $\langle \cos\theta(s) \rangle$, where θ is the angle between bond vectors separated by s segments along the backbone. For an ideal semiflexible chain,

$$\langle \cos\theta(s) \rangle \propto \exp\left(-\frac{s}{l_p}\right), \tag{4}$$

where l_p is the persistence length [35].

The relationship between the persistence length and the number of grafts in bottle-brush polymers

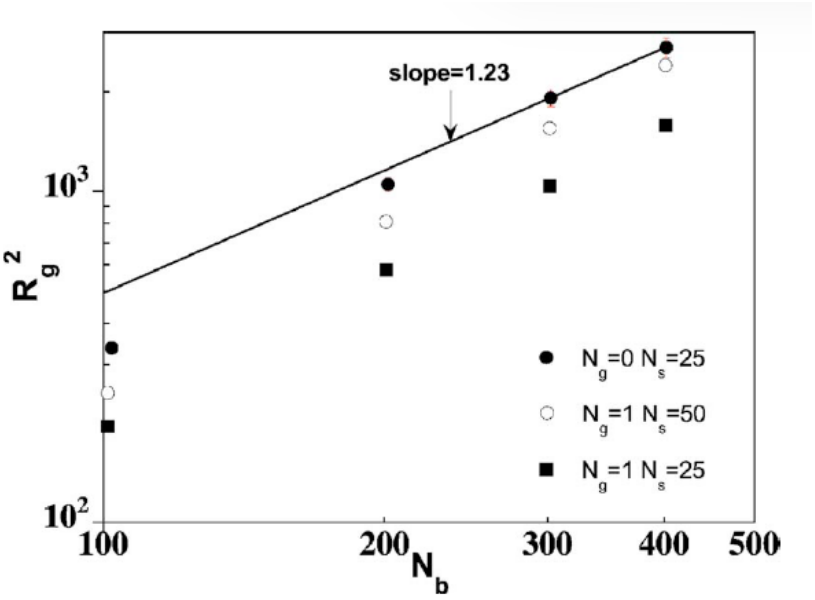

Figure 5: Log-log plot showing the relationship between the radius of gyration and the polymerization degree of the backbone, for $N_b = [102, 202, 302, 402]$. The solid line represents a power-law fit to the last two data points, with the indicated slope [35].

remains underexplored in the literature. However, some consistency with molecular dynamics simulations has been observed [3], while calculating the persistence length for several sidechain lengths ranging from $N_g = 24$ to $N_g = 55$ with a backbone length of $N_b = 200$ (see Figure 6). As N_g increases, the backbone's rigidity initially shows a moderate rise up to a certain sidechain length ($N_g \approx 40$), following $l_p \propto N_g^{3/5}$. Beyond this point, the rigidity increases more significantly, following $l_p \propto N_g^{15/8}$.

This result aligns with Fredrickson's analysis [11] which suggest that, in the high-coverage limit or with longer side-chain lengths, the bottle-brush adopts a toroidal configuration, leading to a stronger dependence of $l_p \propto N_g^{15/8}$ but also matches another study [9], where the $15/8$ dependence was predicted to become relevant only for sufficiently long side-chains. For shorter grafted side-chains, previous studies [32, 14] indicated that l_p exhibits a weaker dependence on N_g, as verified in this research [3].

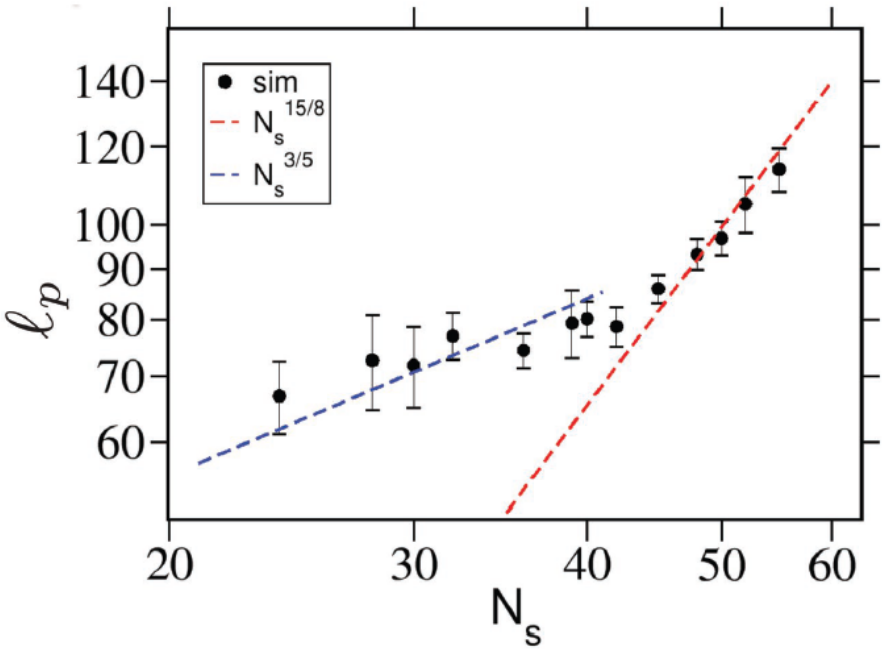

Figure 6: Log-log plot showing the relationship between the persistence length and the sidechain lengths for $24 \leq N_s \leq 55$ at $N_b = 200$, where N_s represents N_g in the original paper [3].

3 Methods

Numerous studies have concentrated on designing and analyzing BBPs through various experimental and computational methods to understand their conformational properties under different conditions such as in solutions, on surfaces, and in melt states [20]. Although experimental approaches provide valuable insights, limitations in resolution hinder a deep understanding of molecular-level relationships and short-time-scale behaviors. Consequently, computational methods have become pivotal, leveraging sophisticated algorithms and improved computational capabilities to accurately predict BBPs structures and properties. Molecular simulations offer a particularly advantageous tool, facilitating the validation of theoretical predictions and providing insights into the behavior of BBPs at the molecular level [16, 17].

3.1 Molecular Dynamics

Molecular dynamics (MD) simulations are among the most widely used particle-based methods, as they provide a route to understanding the dynamical properties of systems, including transport coefficients, time-dependent responses to perturbations, rheological properties, and spectra [2].

Molecular dynamics simulations involve numerically solving Newton's equations (Eq. 5) of motion for each particle in a system, utilizing a set of initial conditions. These initial conditions include the initial positions $\{\mathbf{r}_i\}$ and velocities $\{\frac{d\mathbf{r}_i}{dt}\}$ of the particles. Additionally, the simulations account for inter-particle interactions, denoted by $\mathbf{F}_i(t)$, where i ranges from 1 to n for a system comprising n particles. By integrating these equations over time, molecular dynamics simulations generate trajectories that depict the evolving behavior and interactions of molecules within the system [2].

$$\begin{aligned} m_i \frac{d^2 r_i(t)}{dt^2} &= F_i(t) \\ F_i(t) &= -\frac{\partial U}{\partial r_i} \end{aligned} \tag{5}$$

Using the Verlet algorithm, the position of a particle at time t is expanded to the second order in terms of the timestep δt. This allows us to calculate the position of the particle at time $t+\delta t$. This process is repeated for all particles, and the new positions are stored, enabling the calculation of positions at time $t+2\delta t$. By running the simulation over a large number of sufficiently small timesteps, we can achieve a complete time evolution of the positions of the particles within the system [27].

The interaction potentials, also known as force field interactions, can be divided as bonded and nonbonded interactions [20].

$$\begin{aligned} U &= U_{\text{bonded}} + U_{\text{nonbonded}} \\ U_{\text{bonded}} &= \sum_{\text{bonds}} k_b (b-b_0)^2 + \sum_{\text{angles}} k_\theta (\theta-\theta_0)^2 + \sum_{\text{dihedrals}} \frac{k_\phi}{2}(1+\cos(n\varphi-\varphi_0)) + \sum_{\text{impropers}} k_\psi (\psi-\psi_0)^2 \\ U_{\text{nonbonded}} &= \sum_{i=1}^{n-1}\sum_{j>i}^{n} \frac{q_i q_j}{4\pi\varepsilon r_{ij}} + \sum_{i=1}^{n-1}\sum_{j>i}^{n} 4\varepsilon \left[\left(\frac{\sigma}{r_{ij}}\right)^{12} - \left(\frac{\sigma}{r_{ij}}\right)^{6} \right] \end{aligned} \tag{6}$$

BBPs simulations often employ coarse-grained (CG) models to study the overall conformations of these polymers while minimizing computational expense. By omitting detailed interatomic calculations, CG models streamline the analysis of complex structures [20].

3.2 Model

In this study, we utilized the bead-spring polymer model [6] within the LAMMPS Molecular Dynamics Simulator for BBPs simulations [33]. The solvent was treated as an implicit good solvent, balancing computational efficiency and accuracy [26, 30].
Particle interactions are modeled using a soft pair potential with a coefficient of 1.0, while the bonds between particles are described by the FENE (Finite Extensible Nonlinear Elastic) potential. Special bonds and angles are also treated using the FENE and harmonic styles, respectively. The FENE potential is given by:

$$V_{\text{FENE}}(r) = -\frac{1}{2}kR_0^2 \ln\left[1 - \left(\frac{r}{R_0}\right)^2\right], \quad \text{for } r \leq R_0 \tag{7}$$

where $k = \frac{30\varepsilon}{\sigma^2}$ and $R_0 = 1.5\sigma$.

Initially, pair interactions are set to zero, and a variable prefactor is defined to linearly ramp from 0 to 300. This ramp is applied to the soft potential via the `fix adapt` command, dynamically adjusting interaction strength during the initial equilibration phase. Bond coefficients are set with a stiffness of 30.0, a maximum bond extension of 1.5, and FENE parameters of 1.0. Angle coefficients are defined with a harmonic potential, which varies depending on the polymer's stiffness, with equilibrium angles set to 180 degrees.
The equations of motion are integrated using the velocity Verlet algorithm with a time step of 0.005 and a damping parameter set to 100 times the timestep. The system is equilibrated using the NVT ensemble, with the temperature maintained at 1.0 in Lennard-Jones units to minimize thermodynamic fluctuations. The equilibration phase runs for 10,000 timesteps following the `fix nvtSoft` setup. To determine if the system has indeed equilibrated, we monitor several thermodynamic properties such as total energy, potential energy, kinetic energy, temperature, and pressure. These properties are printed every 1000 steps, and equilibration is confirmed when these quantities fluctuate around stable values without any noticeable drift or trend over time. Additionally, visual inspection of the system's trajectory can provide further confirmation that the system has reached equilibrium. If these properties are stable, the system is considered equilibrated and ready for production runs.
After initial equilibration, the interactions switch to a Lennard-Jones potential [2] with a cutoff set at $2^{1/6}\sigma$, and both the interaction energy ε and particle size σ are set to 1.0. The Lennard-Jones potential is expressed as:

$$U_{\text{LJ}}(r) = 4\varepsilon\left[\left(\frac{\sigma}{r}\right)^{12} - \left(\frac{\sigma}{r}\right)^{6}\right] \tag{8}$$

Trajectory data was recorded both linearly and logarithmically for subsequent shape and mean square displacement (MSD) analysis.

The size of the simulation box is calculated based on the lengths of the backbone (N_b) and side chains (N_g), the number of chains (N) (we will consider 10 chains to have a better average of the measurements), and the desired density (ρ). Specifically, the `box_size` is determined by first computing the

total mass of all chains using the formula:

$$M = ((N_b \times N_g) + N_b) \times N \tag{9}$$

In simulations, a cubic box of volume $V = D^3$ is typically used, and unless surface effects are under investigation, periodic boundary conditions are commonly applied [27]. The density of the system, ρ, is defined by the equation $\rho = \frac{M}{V}$, where ρ is set to 0.01 for a dilute solution. Therefore, the volume V can be computed as:

$$V = \frac{M}{\rho} \tag{10}$$

Finally, taking the cube root of this volume provides the length of each side of the cubic simulation box, ensuring the system maintains the specified density:

$$\text{box\_size} = \left(\frac{M}{\rho}\right)^{1/3} \tag{11}$$

3.3 Analysis

The computational workflow and data management for this report were supported by the `signac` data management framework and the additional `signac-flow` Python package [1, 5, 25]. Analysis of the trajectory files from the MD simulations and calculation of the persistence length was performed using the `MDAnalysis` Python package [13, 19]. The visualization and plotting of the obtained data were performed using the `matplotlib` and `Seaborn` packages [29]. Numerical fitting of the obtained data was carried out through non-linear least square minimization using the `lmfit` Python package, ensuring more reliable and robust fits by considering confidence intervals [23]. Additional qualitative analysis was performed on visual snapshots of the simulated systems using the `OVITO` visualization software [31].

4 Results and Discussion

As explained in Chapter 2, the principal characteristics and scaling laws governing the behavior of flexible BBPS were discussed. To understand the molecular shape and characteristics of semi-flexible bottlebrush polymers, stiffness is introduced to these polymers. This transformation from flexible to semi-flexible bottlebrush polymers is achieved by incorporating angular potentials along the backbone and side chains, which impose preferred angles between connected atoms through the LAMMPS command `angle_style harmonic` [33]. The harmonic angle style uses the potential shown in Equation 12 to maintain an extended configuration for both the backbone and side chains [21].

$$E = k(\theta - \theta_0)^2 \tag{12}$$

where k is the prefactor indicating stiffness, θ_0 is the equilibrium angle of 180° and θ is the current angle between the three atoms.
A stiffness value (k) ranging from 2 to higher values is applied to all bond types in the simulations to explore the characteristics of semi-flexible BBPs (Figure 7). Higher k values make the system more resistant to deviations from the equilibrium angle, requiring more energy to bend away from 180°.

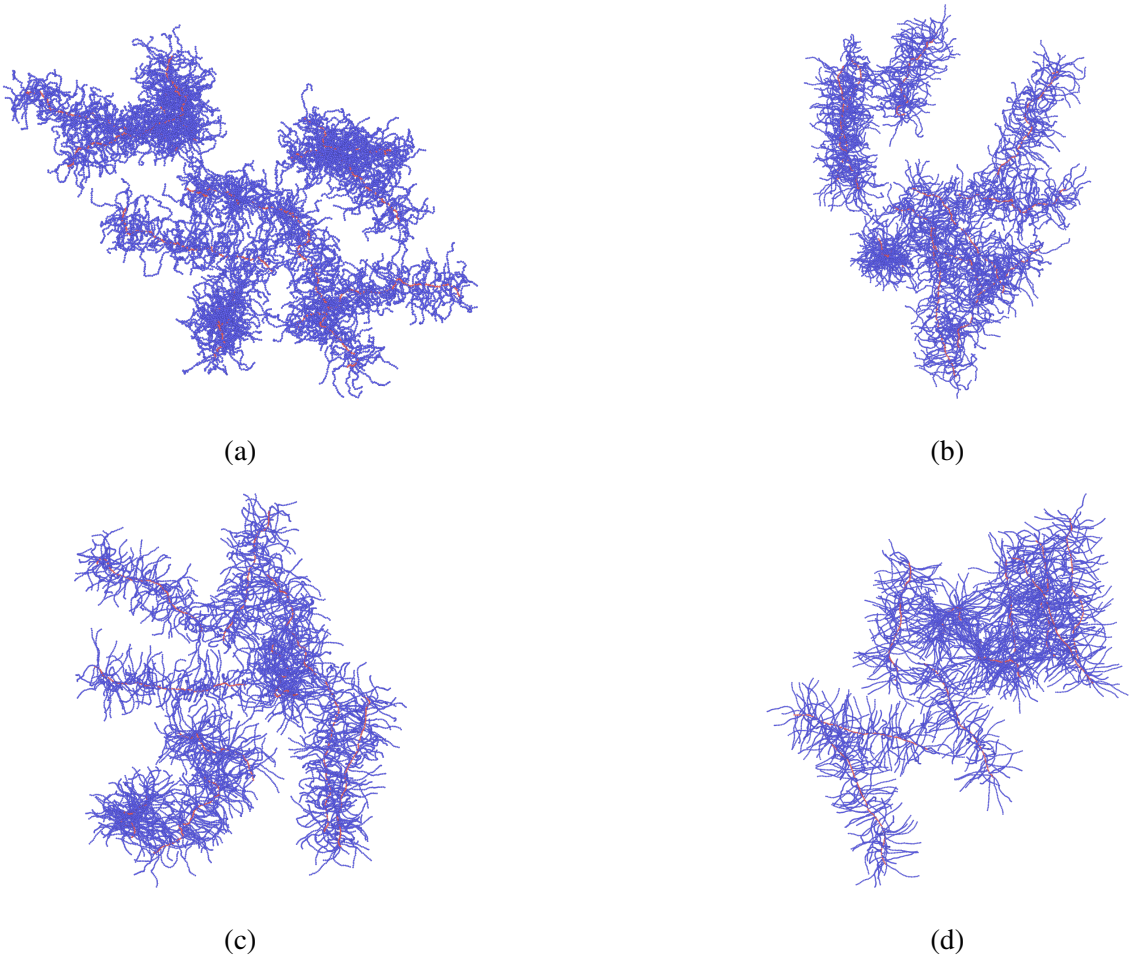

(a) (b) (c) (d)

Figure 7: Front simulation snapshots obtained with `OVITO` of 10 semi-flexible bottlebrush polymers with $N_b = 102$ and $N_g = 25$, respectively, with stiffness values of (a) $k = 2$, (b) $k = 6$, (c) $k = 10$, and (d) $k = 30$.

4.1 Radius of Gyration in Semi-flexible Bottlebrush Polymers

An important characteristic to explore when the stiffness of the polymer increases is the radius of gyration (R_g). As discussed in Section 2.2.1, the relationship between the radius of gyration and the backbone length (N_b) is described by the scaling law $R_g \propto N_b^{\alpha}$, with α varying between 0.6 and 0.7.

In this study, we fixed the number of grafted side chains (N_g) at 25 while varying the backbone length (N_b) and considering four values (102, 202, 303, and 402), consistent with the approach in the referenced study [35]. The stiffness was modulated by varying the parameter k and considering $k = 2, 6, 10$ and 30.

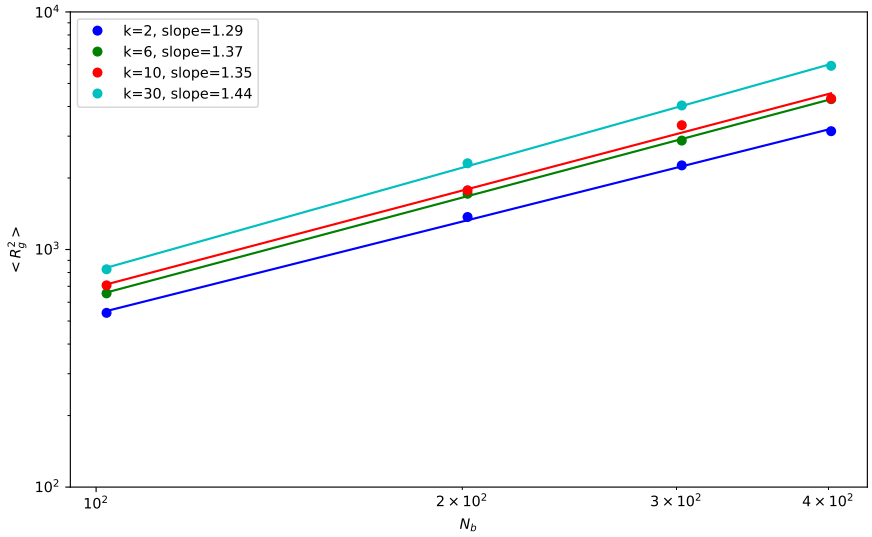

Figure 8: The relationship between the squared radius of gyration $\langle R_g^2 \rangle$ and the backbone length N_b for $k = 2, 6, 10$ and $k = 30$. The different degrees of rigidity are represented by various colors, and the slopes are calculated using the least squares method in log-log space.

The resulting plot (see Figure 8) illustrate the relationship between $\langle R_g^2 \rangle$ and N_b for different values of k (2, 6, 10 and 30). It is evident from the graphs that as N_b increases, R_g increases in a manner that closely follows the scaling law, with α ranging from 0.6 to 0.7. This indicates a consistent relationship between the radius of gyration and the backbone length.
Moreover, the plot reveal that with higher values of k, indicating increased stiffness, the slope of the log-log plot becomes steeper. This implies a stronger relationship between R_g and N_b, suggesting that α slightly exceeds 0.7. This trend demonstrates that, as the polymer becomes stiffer, the radius of gyration scales more significantly with the backbone length, reinforcing the observed scaling behavior.

4.2 Persistence Length in Semi-flexible Bottlebrush Polymers

The persistence length is a measure of the distance over which the polymer backbone retains its orientation. The bond correlation function $C(x)$ exhibits an exponential decay as a function of the distance x along the polymer backbone. To better understand the behavior of the persistence length in stiffer polymers, this study considers a fixed backbone length of $N_b = 200$ while varying the side

chain lengths ($24 \leq N_g \leq 55$). For different stiffness values ($k = 2$, $k = 6$, $k = 10$ and $k = 30$), the bond correlation function $C(x)$ was plotted and the persistence length was extracted. As mentioned in Section 2.2.2, long side chains can significantly impact the rigidity of the polymer. This effect is amplified by increasing the stiffness of the polymer.

Orientation correlations of bonds within a chain are investigated using Equation (4) and shown in Figure 9. In the autocorrelation function, the exponential decay is governed by the persistence length l_p and for a finite rod, this relation expects $l_p = \infty$ [4]. From the second bond in the chain, the correlation starts to decay from unity. The semi-log plots reveal that as the side chain lengths increase, the persistence length also increases, a phenomenon predicted in previous studies [3, 11, 9, 32, 14] and reconfirmed here with the added variable of increased stiffness (k). For relatively short side chains (e.g., $N_g = 25$ and 30), the plot shows an exponential decay of $C(x)$. However, for longer side chains (e.g., $N_g = 45, 50$, and 55), an upward deviation reveals that the bond correlation function fits an exponential decay more closely, indicating that bond orientation correlations persist over longer distances.

In general, the observed behavior confirms that higher stiffness values (k) lead to significantly larger persistence lengths, demonstrating that the polymer maintains its directional orientation over greater distances and exhibits a near-linear conformation. The analysis shows that increasing both the side chain lengths and the stiffness of the polymer leads to significantly larger persistence lengths, which aligns with theoretical predictions and previous studies. This indicates that stiffer polymers with longer side chains maintain their directional orientation over greater distances, resulting in more linear conformations.

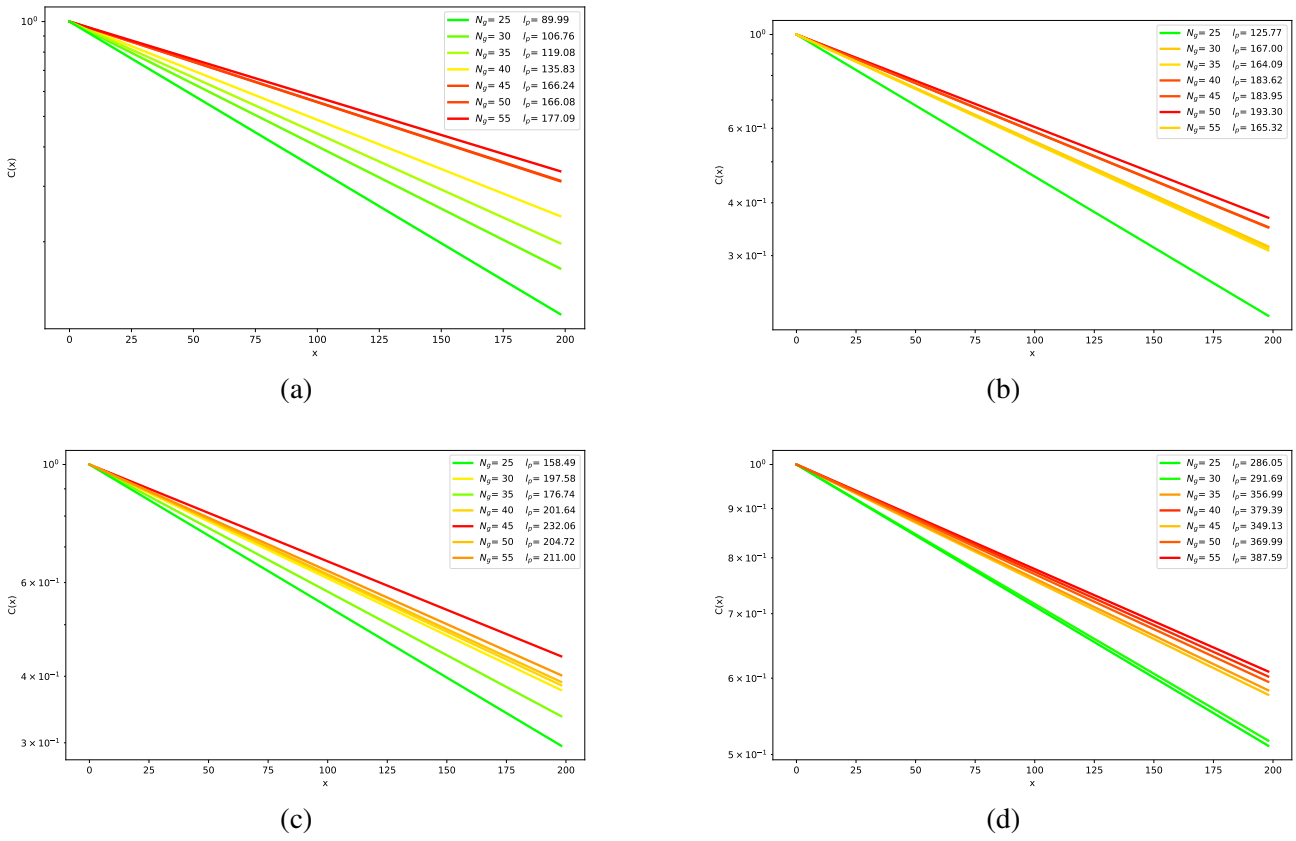

Figure 9: Bond correlation function $C(x)$ for different side chain lengths (N_g) and stiffness values: (a) $k = 2$, (b) $k = 6$, (c) $k = 10$, and (d) $k = 30$.

5 Conclusion

This study reviewed the experimental progress in understanding the conformational evolution of flexible bottlebrush polymers in dilute solutions, and extended this understanding to semi-flexible bottlebrushes. Molecular dynamics simulations were employed to explore the conformational properties and static structure of these highly branched polymers using a coarse-grained model.
The analysis focused on key dependencies between conformational properties and structural parameters, particularly the radius of gyration and the persistence length, considering varying degrees of polymerization.

Regarding the radius of gyration, theoretical, experimental, and simulation studies consistently highlight a strong correlation with increasing values of N_b [35], which is further pronounced with the introduction of polymer stiffness, confirming theoretical predictions.
The study also investigated the persistence length, noting prior findings that indicate a weaker dependence on short side chains and a stronger correlation with longer side chains [3, 11, 9, 32, 14]. This investigation specifically addressed how persistence length varies with side chain length and polymer rigidity. The results demonstrate not only an increase in persistence length with longer side chains, but also significant sensitivity to polymer stiffness. The bond correlation function $C(x)$ exhibits an exponential decay, and our findings indicate that this decay is slower for stiffer polymers, resulting in longer persistence lengths. This suggests that stiffer polymers maintain their directional orientation over greater distances, which aligns with theoretical predictions and previous studies.
In conclusion, this study contributes to a deeper understanding of how structural modifications, such as side chain length and polymer stiffness, influence the conformational properties of bottlebrush polymers. The results from our bond correlation function analysis reinforce the theoretical predictions and experimental observations, highlighting the significant impact of polymer stiffness and side chain length on the persistence length and overall conformation of the polymers.

In future works, by systematically altering conformational and structural parameters, we can gain a deeper understanding of the complex interplay between these factors and polymer rigidity. Additionally, introducing stiffness to both the backbone and/or side chains offers a promising pathway for further exploration. Specifically, examining the impact of varying degrees of stiffness in different segments of the polymer can provide insights into how local and global conformations are affected. This can help to identify critical thresholds at which the polymer transitions from flexible to semi-flexible or rigid behavior.
Moreover, these future studies can employ advanced simulation techniques and experimental methods to validate theoretical predictions and refine models. By extending the investigation to include temperature variations, solvent interactions, and different polymer architectures, a more comprehensive picture of polymer behavior can be developed. These efforts will not only enhance our fundamental understanding of polymer science but also inform the design of new materials with tailored mechanical and structural properties, suitable for specific applications in areas such as biomedicine, nanotechnology, and materials engineering.
Thus, the ongoing exploration of how structural modifications and stiffness contribute to polymer rigidity holds significant potential for advancing both theoretical knowledge and practical applications in polymer research.

Bibliography

[1] Carl S Adorf, Paul M Dodd, Vyas Ramasubramani, and Sharon C Glotzer. Simple data and workflow management with the signac framework. *Computational Materials Science*, 146:220–229, 2018.

[2] Michael P Allen et al. Introduction to molecular dynamics simulation. *Computational soft matter: from synthetic polymers to proteins*, 23(1):1–28, 2004.

[3] Debarati Chatterjee and Thomas A Vilgis. Scaling laws of bottle-brush polymers in dilute solutions. *Macromolecular Theory and Simulations*, 25(6):518–523, 2016.

[4] Peter Cifra. Differences and limits in estimates of persistence length for semi-flexible macromolecules. *Polymer*, 45(17):5995–6002, 2004.

[5] Bradley Dice, Brandon Butler, Vyas Ramasubramani, Alyssa Travitz, Michael Henry, Hardik Ojha, Kelly Wang, Carl Adorf, Eric Jankowski, and Sharon Glotzer. Signac: Data management and workflows for computational researchers. In *Proceedings of the Python in Science Conference*, 2021.

[6] Masao Doi. *Introduction to polymer physics*. Oxford university press, 1996.

[7] Sarit Dutta, Matthew A Wade, Dylan J Walsh, Damien Guironnet, Simon A Rogers, and Charles E Sing. Dilute solution structure of bottlebrush polymers. *Soft Matter*, 15(14):2928–2941, 2019.

[8] Stefano Elli, Fabio Ganazzoli, Edward G Timoshenko, Yuri A Kuznetsov, and Ronan Connolly. Size and persistence length of molecular bottle-brushes by monte carlo simulations. *The Journal of chemical physics*, 120(13):6257–6267, 2004.

[9] Laurent Feuz, Frans AM Leermakers, Marcus Textor, and Oleg Borisov. Bending rigidity and induced persistence length of molecular bottle brushes: A self-consistent-field theory. *Macromolecules*, 38(21):8891–8901, 2005.

[10] Paul J Flory and M Volkenstein. Statistical mechanics of chain molecules, 1969.

[11] Glenn H Fredrickson. Surfactant-induced lyotropic behavior of flexible polymer solutions. *Macromolecules*, 26(11):2825–2831, 1993.

[12] Sean Gill, Thomas N Wight, and Charles W Frevert. Proteoglycans: key regulators of pulmonary inflammation and the innate immune response to lung infection. *The Anatomical Record: Advances in Integrative Anatomy and Evolutionary Biology*, 293(6):968–981, 2010.

[13] Richard J Gowers, Max Linke, Jonathan Barnoud, Tyler John Edward Reddy, Manuel N Melo, Sean L Seyler, Jan Domanski, David L Dotson, Sébastien Buchoux, Ian M Kenney, et al. Mdanalysis: a python package for the rapid analysis of molecular dynamics simulations. Technical report, Los Alamos National lab.(LANL), Los Alamos, NM (United States), 2019.

[14] Hsiao-Ping Hsu, Wolfgang Paul, and Kurt Binder. Polymer chain stiffness vs. excluded volume: A monte carlo study of the crossover towards the worm-like chain model. *Europhysics Letters*, 92(2):28003, 2010.

[15] Gregory D Jay. Characterization of a bovine synovial fluid lubricating factor. i. chemical, surface activity and lubricating properties. *Connective tissue research*, 28(1-2):71–88, 1992.

[16] Zhifeng Jing, Chengwen Liu, Sara Y Cheng, Rui Qi, Brandon D Walker, Jean-Philip Piquemal, and Pengyu Ren. Polarizable force fields for biomolecular simulations: Recent advances and applications. *Annual Review of biophysics*, 48:371–394, 2019.

[17] Soumil Y Joshi and Sanket A Deshmukh. A review of advancements in coarse-grained molecular dynamics simulations. *Molecular Simulation*, 47(10-11):786–803, 2021.

[18] Zili Li, Miao Tang, Shuang Liang, Mingyue Zhang, Gill M Biesold, Yanjie He, Shu-Meng Hao, Woosung Choi, Yijiang Liu, Juan Peng, et al. Bottlebrush polymers: From controlled synthesis, self-assembly, properties to applications. *Progress in Polymer Science*, 116:101387, 2021.

[19] Naveen Michaud-Agrawal, Elizabeth J Denning, Thomas B Woolf, and Oliver Beckstein. Mdanalysis: a toolkit for the analysis of molecular dynamics simulations. *Journal of computational chemistry*, 32(10):2319–2327, 2011.

[20] Esmat Mohammadi, Soumil Y Joshi, and Sanket A Deshmukh. A review of computational studies of bottlebrush polymers. *Computational Materials Science*, 199:110720, 2021.

[21] Bernard Monasse and Frédéric Boussinot. Determination of forces from a potential in molecular dynamics. *arXiv preprint arXiv:1401.1181*, 2014.

[22] Rikkert J Nap and Igal Szleifer. Structure and interactions of aggrecans: statistical thermodynamic approach. *Biophysical journal*, 95(10):4570–4583, 2008.

[23] Matthew Newville, Till Stensitzki, Daniel B Allen, Michal Rawlik, Antonino Ingargiola, and Andrew Nelson. Lmfit: Non-linear least-square minimization and curve-fitting for python. *Astrophysics Source Code Library*, pages ascl–1606, 2016.

[24] Jarosław Paturej, Sergei S Sheiko, Sergey Panyukov, and Michael Rubinstein. Molecular structure of bottlebrush polymers in melts. *Science advances*, 2(11):e1601478, 2016.

[25] Vyas Ramasubramani, Carl Adorf, Paul Dodd, Bradley Dice, and Sharon Glotzer. signac: A python framework for data and workflow management. In *Proceedings of the Python in Science Conference*, 2018.

[26] Govardhan Reddy and Arun Yethiraj. Implicit and explicit solvent models for the simulation of dilute polymer solutions. *Macromolecules*, 39(24):8536–8542, 2006.

[27] Michael Rubinstein and Ralph H Colby. *Polymer physics*. Oxford university press, 2003.

[28] Sergei S Sheiko, Brent S Sumerlin, and Krzysztof Matyjaszewski. Cylindrical molecular brushes: Synthesis, characterization, and properties. *Progress in Polymer Science*, 33(7):759–785, 2008.

[29] Ali Hassan Sial, Syed Yahya Shah Rashdi, and Abdul Hafeez Khan. Comparative analysis of data visualization libraries matplotlib and seaborn in python. *International Journal*, 10(1):45, 2021.

[30] Justin R Spaeth, Ioannis G Kevrekidis, and Athanassios Z Panagiotopoulos. A comparison of implicit-and explicit-solvent simulations of self-assembly in block copolymer and solute systems. *The Journal of chemical physics*, 134(16), 2011.

[31] Alexander Stukowski. Visualization and analysis of atomistic simulation data with ovito–the open visualization tool. *Modelling and simulation in materials science and engineering*, 18(1):015012, 2009.

[32] Panagiotis E Theodorakis, Hsiao-Ping Hsu, Wolfgang Paul, and Kurt Binder. Computer simulation of bottle-brush polymers with flexible backbone: Good solvent versus theta solvent conditions. *The Journal of chemical physics*, 135(16), 2011.

[33] Aidan P Thompson, H Metin Aktulga, Richard Berger, Dan S Bolintineanu, W Michael Brown, Paul S Crozier, Pieter J In't Veld, Axel Kohlmeyer, Stan G Moore, Trung Dac Nguyen, et al. Lammps-a flexible simulation tool for particle-based materials modeling at the atomic, meso, and continuum scales. *Computer Physics Communications*, 271:108171, 2022.

[34] Rafael Verduzco, Xianyu Li, Stacy L Pesek, and Gila E Stein. Structure, function, self-assembly, and applications of bottlebrush copolymers. *Chemical Society Reviews*, 44(8):2405–2420, 2015.

[35] Arun Yethiraj. A monte carlo simulation study of branched polymers. *The Journal of chemical physics*, 125(20), 2006.

[36] Mo Zhu, Xuejun Pan, Tao Zheng, and Lian-Wei Li. Research progress on the conformational property of comb-like polymers in dilute solution. *Soft Matter*, 2024.